The Cenomanian heterozoan carbonates in the north-central Alborz, north-east Kelardasht, north Iran

Mohammad Ali KAVOOSI[1, *] and Neda EZOJI[2]

[1] Exploration Directorate of National Iranian Oil Company (NIOCEXP), Khodami Street, NE Sheikh Bahaei Square, PO Box 19395-6669, Tehran, Iran

[2] Ministry of Education, School of Professor Hessabi, Sadeghieyeh Square, Tehran, Iran

Detailed field surveys, petrographic investigation and SEM and EDS analyses have been used to evaluate Cenomanian glauconitic heterozoan carbonates in north-east Kelardasht, north-central Alborz, north Iran. Lithofacies and microfacies analyses led to recognition of six microfacies types related to the inner-, mid- and outer-ramp facies belts of a carbonate ramp. The heterozoan nature of these carbonates is inferred from a predominance of echinoderms associated with calcispheres, planktonic foraminifers, a lack of ooid grains, and a low carbonate production rate, together with a high content of glauconite grains and prevailing high-Mg calcite mineralogy. Petrographic and SEM studies reveal that glauconite filling skeletal grains retains the shape and morphology of host grains, signifying an authigenic origin at low sedimentation rates and slightly reducing conditions. SEM images show cauliflower and rosette structures associated with well-developed lamellae indicating an authigenic origin of evolved glauconite grains. Our findings are compatible with a nutrient-rich waters and palaeoecological stress related to relative sea-level rise and eutrophic conditions, which contributed to the generation of these heterozoan carbonates despite the hot greenhouse conditions during the Cenomanian in the north-central Alborz Mountains.

Key words: heterozoan carbonates, authigenic glauconite, Cenomanian, north-east Kelardasht, Iran.

INTRODUCTION

The Cenomanian (93.9–100.5 Ma) was a time interval associated with relative sea-level rise and greenhouse conditions (e.g., Huber et al., 2018), which led to the drowning of carbonate platforms and deposition of glauconitic sediments related to Oceanic Anoxic Event 2 (OAE 2, e.g., Rudmin et al., 2017; Hairapetian et al., 2018).

Cenomanian glauconitic deposits have been reported from the Central Iran Basin in the Esfahan area (Kennedy et al., 1979; Hairapetian et al., 2018), the Kopeh Dagh Basin in north-east Iran (Jafarzadeh et al., 2020), in Devon, south-west England (e.g., Carson and Crowley, 1993), in the Cretaceous deposits of south-east Spain (Jimenez-Millan et al., 1998), and in the Lower Cenomanian Bahariya Formation in the Western Desert of Egypt (Baioumy et al., 2021). Glauconite has been reported from Cretaceous marine deposits of the Tethyan belt (e.g., Bansal et al., 2020; Jafarzadeh et al., 2020).

The heterozoan carbonates (James, 1997) comprise an association of light-independent, suspension-feeding, and heterotrophic fauna including echinoderms, calcispheres, planktonic foraminifers, bryozoans and pelecypods (foramol association). Factors responsible for the occurrence of heterozoan carbonates are climate, geotectonic setting, temperature, salinity, water depth, trophic conditions, oxygen level, CO_2 concentrations, Mg/Ca ratio of sea-water, alkalinity, morphology and bathymetry of the sea-floor, substrate, and transparency of the sea water (Tucker and Wright, 1990; Pomar et al., 2005; Westphal et al., 2010). Climate and geotectonic setting control temperature, water circulation patterns, turbulence, as well as nutrient supply (Tucker and Wright, 1990).

The Cenomanian lithostratigraphic unit of the Kelardasht and Chalus counties (Figs. 1–3) is marked by thin- to medium-bedded glauconitic limestones comprising heterozoan carbonates composed mainly of echinoderms, red algae, bryozoans, planktonic foraminifers, glauconite, associated with a few sparse phosphate grains and subordinate quartz grains. Silt-to sand-sized quartz and basaltic lithoclasts within the succession indicate weathering of nearby lands and influx of siliciclastic sediment into the depositional setting.
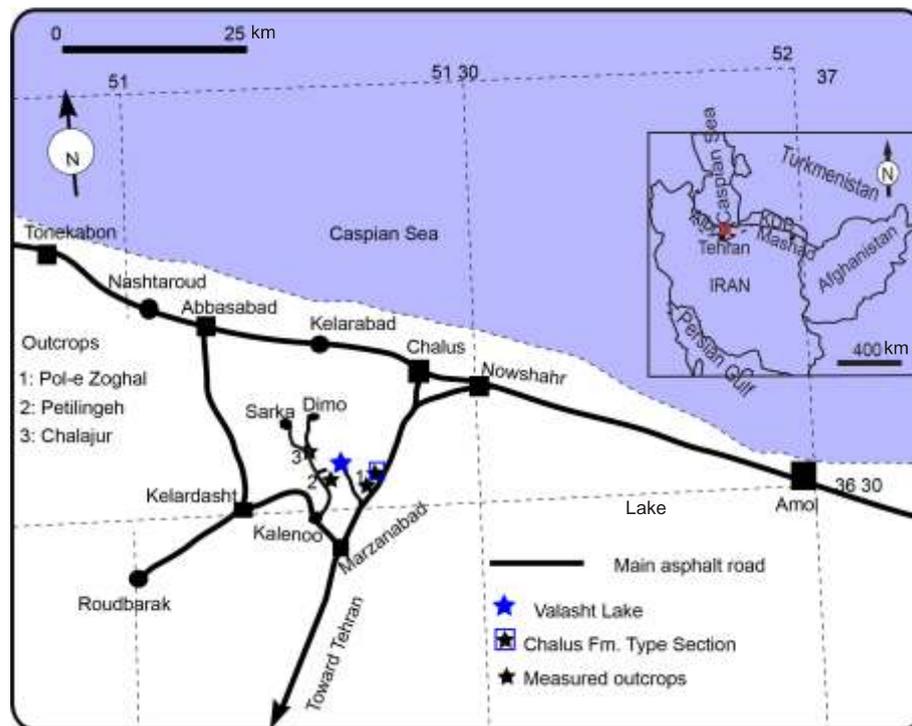
Fig. 1. Location map of the exposed sections studied, located in the north-central Alborz Mountain Range, in the Chalus and Kelardasht counties, N Iran

Pelagic facies comprising glauconite grains among other indicators may suggest deposition accompanied by a sudden sea-level rise and an increment of nutrient related to upwelling currents (e.g., Yilmaz et al., 2018). Relative sea-level rise together with a low sedimentation rate provide suitable conditions for glauconite to form (e.g., Nichols, 2009; Rudmin et al., 2017).

The study was carried out in the north-central Alborz Mountain range, in the north-east Kelardasht county, west of the Mazandaran Province, north Iran (Figs. 1 and 2). To date, microfacies analysis and depositional environments of the Cenomanian succession in the study area (Figs. 1 and 2) has remained poorly known except for Ezoji (2002) and Abbaspour--Tehrani (2014).

Microfacies analysis was undertaken to interpret the Cenomanian heterozoan carbonates in the north-central Alborz. An understanding of the factors controlling the carbonate contribution and production would be useful to evaluate the interaction of the depositional setting and tectonic, climate, and sea-level changes (Kavoosi and Ezoji, 2018). The study examines the factors which controlled the temporal and spatial distribution of these glauconitic limestones during the Cenomanian.

GEOLOGICAL SETTING

The Alborz is a 1500 km long mountain range and an active fold-thrust belt across northern Iran, extending from the Lesser Caucasus of Armenia in the north-west to the Paropamisus Mountains of Northern Afghanistan, flanking in its central part the southern coast of the Caspian Sea (Alavi, 1996; Allen et al., 2003; Guest et al., 2007; Zanchi et al., 2009; Yassaghi and Naeimi, 2010; Kangi et al., 2010), still documenting seismic activity (Mattei et al., 2017). The central Alborz range underwent extensional movements related to distal effects of the Cimmerian Orogeny in the South Caspian back-arc basin (Fürsich et al., 2005, 2009a, b; Berra et al., 2007; Zanchi et al., 2009; Egan et al., 2009).

The varied geological history of Alborz is recorded by coarse-grained siliciclastics and shallow-platform to basinal carbonate deposits interrupted by alkali-basalt to andesitic volcanic rocks (Fig. 2), as well as by non-depositional periods together with exhumation phases accompanied by fold and thrust activities.

The Mid-Cimmerian event reflects a break-up unconformity and an overall deepening-upwards trend related to extensional movements of the South Caspian Basin during the Middle-Late Jurassic to the Late Cretaceous (Fürsich et al., 2009a; Taheri et al., 2009; Kavoosi and Ezoji, 2018). Extensional movement is inferred from the basin evolution and mafic volcanism during the Late Jurassic, Early and mid-Cretaceous in the study area (Figs. 2 and 3). The volcanic rocks (alkali-basalt, andesite, and pillow lava) most likely indicate a back-arc position and early Cenomanian extensional movements in the north-central Alborz (Egan et al., 2009; Wilmsen et al., 2009).

The lowermost succession of the Cretaceous has is cut by normal fault systems with an E–W to WNW–ESE trend associated with magmatism related to the N–S to NNE–SSW trending extensional systems accompanied by a regional unconformity in northern Iran (Shahidi et al., 2011).

The Cretaceous-Paleocene unconformity can be attributed to beginning of the fold- and thrust-belt activity related to the Laramide Orogenic phase, which affected the southern margin of the South Caspian Basin (Egan et al., 2009; Shahidi et al., 2011; Kavoosi and Ezoji, 2018).
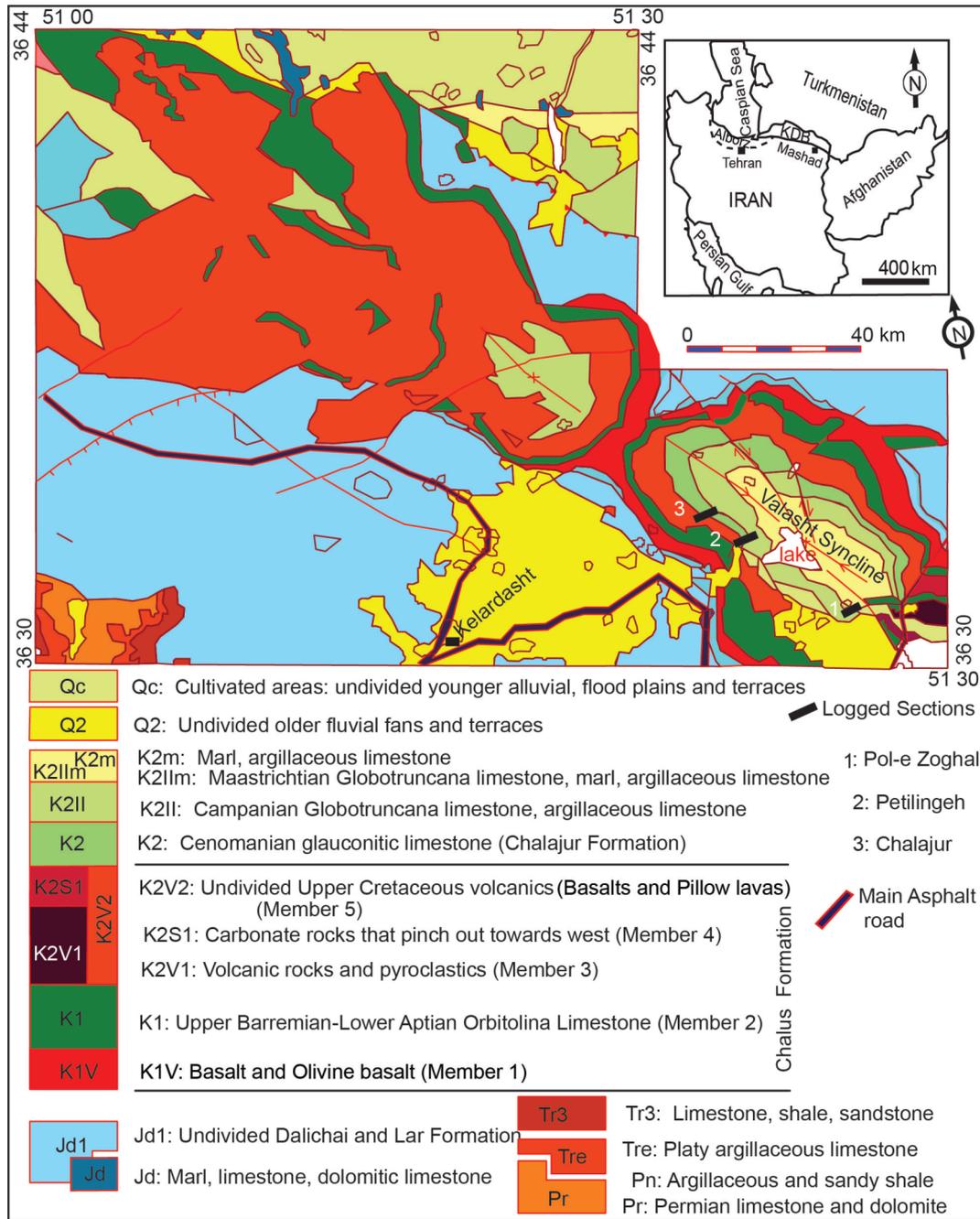
Fig. 2. Modified geological map (1:100,000) of the Chalus region (Vahdati Daneshmand et al., 2001), western Mazandaran Province; Geological Survey of Iran, Tehran

Three exposures, at Pol-e Zoghal, Petilingeh, and Chalajur, are located on the northern and southern flanks of the Valasht Syncline; for interpretation of the references to colour in this figure legend

MATERIAL AND METHODS

The current study of the Cenomanian carbonates in the north-central Alborz (Figs. 2 and 3) is based on integrated detailed field surveys, microfacies analysis and scanning electronic microscopy (SEM) with energy dispersive spectroscopy (EDS). Three exposure sections, at Pol-e Zoghal, Petilingeh and Chalajur were logged and sampled, locate north-east of Kelardasht and south of Chalus (Fig. 1). Lithostratigraphic log-

ging and sedimentological analysis were conducted on very thin- to medium-bedded glauconitic limestones (Fig. 4). Lithofacies were defined based on bedding patterns and sedimentary textures together with skeletal grains and non-carbonate components. The true thickness of the sections was measured with a Jacobs Staff.

Microfacies analysis was performed on 65 thin-sections to complement the field observations and to determine depositional facies. Dunham's nomenclature (1962) was used for the microfacies classification. The grains and matrix percentages
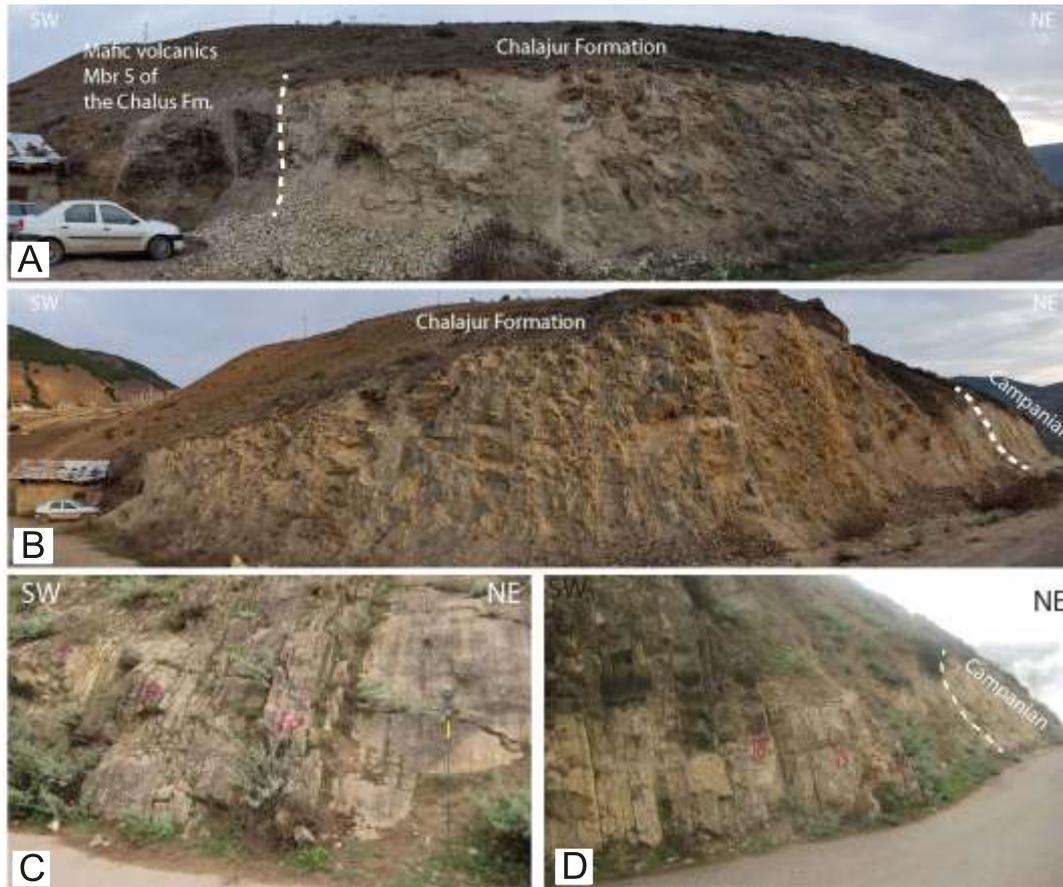
Fig. 3. The newly proposed stratigraphic chart of the north-central Alborz Mountain Range

This stratigraphic chart is constructed based on compilation of previous work (Cartier, 1971; Ezoji, 2002; Robert et al., 2014; Kavoosi and Ezoji, 2018), together with the Chalus geological map, field observations and biostratigraphic dating

were estimated using visual percentage charts (Flügel, 2010). Microfacies analysis was performed using standard microfacies descriptions and the proposed models of Wilson (1997) and Flügel (2010). The prefixes "glauconitic" and "sandy" were added to the names of microfacies with a proportion of >10% glauconite grains, quartz and extraclasts, respectively. In addition, characteristic fabrics and main components were taken into account in the classification of microfacies.

Microfacies types and their depositional environments were determined on the basis of field and petrographic studies, lateral and vertical microfacies changes, and comparison with ancient and recent depositional environments (e.g., Purser, 1973; Tucker and Wright, 1990; Flügel, 2010). The biostratigraphic framework of the successions investigated is mainly based on planktonic foraminifers identified in the thin-sections (Fig. 5).

The SEM and EDS analyses were performed at the Razi Metallurgic Research Centre (RMRC) in Tehran. SEM was used to provide detailed high-resolution images of selected glauconite grains by rastering a focused electron beam across the surface. The EDS was carried out to better understand the formation and chemical characterization of the glauconite grains.

RESULTS

LITHOSTRATIGRAPHY

The lithostratigraphic unit encountered comprises Cenomanian glauconitic carbonates (Figs. 3 and 4). The formation is exposed in the Kelardasht and Chalus counties (Fig. 2). No for-

Fig. 4. Field photo of the Cenomanian Chalajur Formation

A – field photo of the Cenomanian Chalajur Formation that shows its lower nonconformity with the basalts at the Chalajur section; **B** – a panorama of the Chalajur Formation and its upper contact with the Campanian marl and argillaceous limestone; **C** – close-up view of glauconitic limestones and interbedded marl; the red numbers are locations of samples taken for microfacies analysis; **D** – close-up view of glauconitic limestones near the top of the Chalajur Formation and the upper contact with the Campanian argillaceous limestone; note an overall thickening towards the upper part of the formation

mal lithostratigraphic units have yet been proposed for the Upper Cretaceous succession of north-central Alborz (Fig. 3). Based on the International Stratigraphic Guide (Salvador, 1994), we define the Chalajur Formation for the rock unit formerly named the Cenomanian glauconitic limestone (Cartier, 1971). The type locality/type section of the Chalajur Formation is located at the northern end of Chalajur village, comprising 55 m of dominantly greenish-grey to grey, fine-grained, thin- to medium-bedded limestone (Figs. 3 and 4).

The Chalajur Formation is nonconformably underlain by volcanic (alkali basalts) and volcanoclastic rocks of Member 5 of the Chalus Formation (Fig. 4A), and disconformably overlain by the slightly weathered Campanian-Maastrichtian argillaceous limestone and marl (Figs. 3 and 4B, D).

The Chalajur Formation consists of well-bedded glauconitic limestone with subordinate marl interbeds in distinct cyclic packages (Fig. 4C, D). The bedding thickness ranges from a few to twenty centimetres. One characteristic of the cycles is gradational changes in thickness and lithofacies of beds and bed sets (Fig. 4C, D) in the study area (Fig. 1). Glauconite grains are scattered throughout the formation. The glauconite imparts an olive green to greenish grey colour to the Chalajur Formation (Fig. 4A–C).

BIOSTRATIGRAPHY

The biostratigraphic assignment and chronostratigraphic framework are based on a detailed micropalaeontological investigation of planktonic foraminifers in thin-section. The Chalajur Formation, poorly documented from a biostratigraphic point of view (Ezoji, 2002), has been studied using benthic and planktonic foraminifers. Results based on examination of thin-sections led to recognition of several planktonic foraminifers, calcispheres, and heterohelcids (Fig. 5).

Identification of taxa is hampered by widespread recrystallization and neomorphism. For age determination, planktonic foraminifers were studied using the classification schemes of Caron and Premoli Silva (2007) and Petrizzo et al. (2015).

The planktonic foraminifers identified include *Muricohedbergella rischi* (Fig. 5A, B), *Thalmanninella appeninica* (Fig. 5C), *Heterohelix reussi* (Fig. 5D), *Globotruncana lapparenti* (Fig. 5E, F), *Pithonella trejoi* (Fig. 5H, I), and *Whiteinella paradubia* (Fig. 5G)*, associated with *Thalmanninella micheli, Pithonella ovalis, Stomiosphaera sphaerica*.

Stratigraphically, *Thalmanninella brotzeni* occurs slightly earlier than *Thalmanninella globotruncanides* (Caron and Premoli-Silva, 2007). We assigned the Cenomanian age based
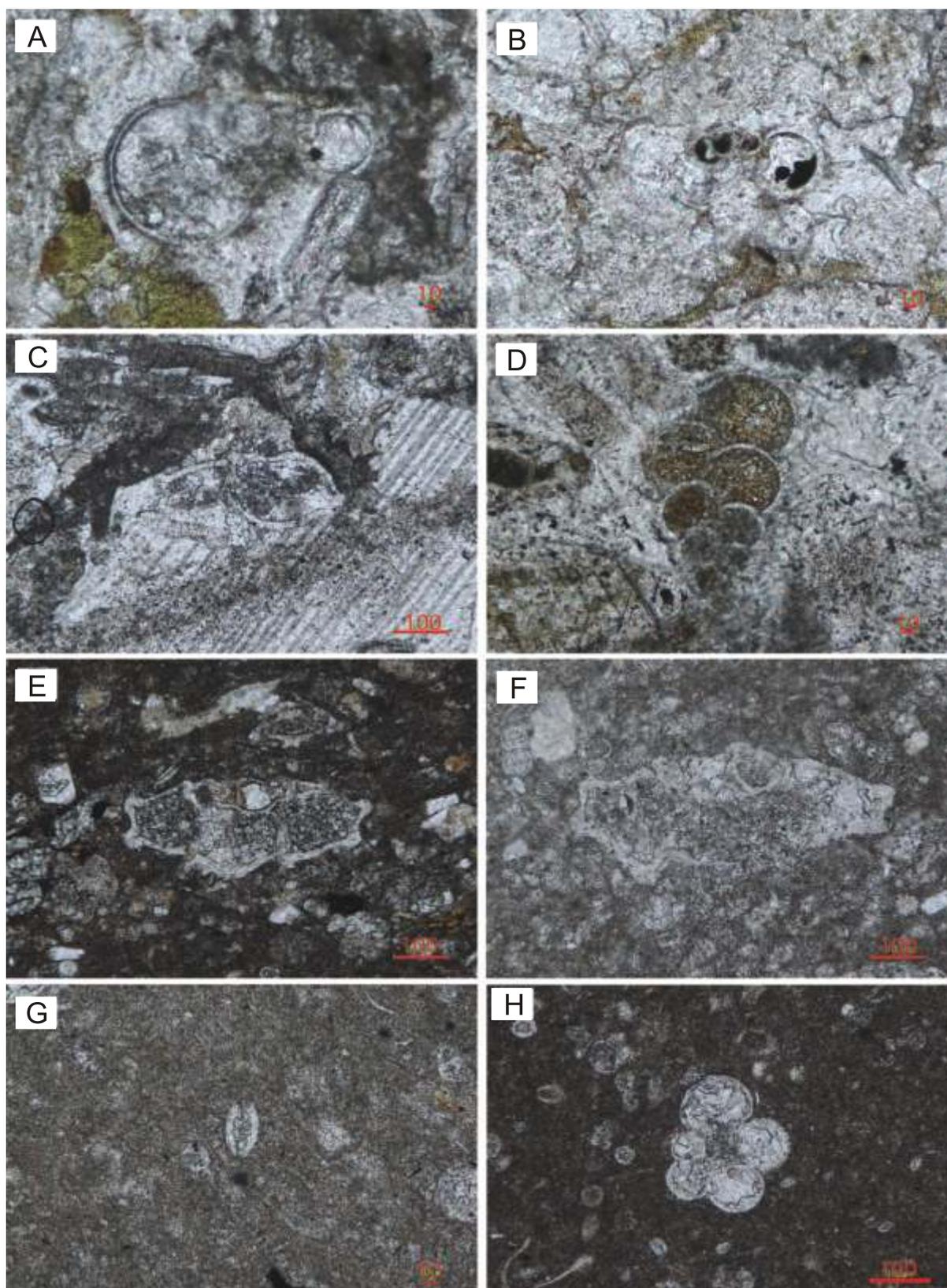
Fig. 5. Photomicrographs of some index microfossils of the Chalajur Formation of Cenomanian age

The iplanktonic foraminifers identified include: **A, B** – *Muricohedbergella rischi* associated with glauconite grains and pyrite,
C – *Thalmanninella appeninica*; **D** – *Heterohelix reussi*; **E, F** – *Globotruncana laparenti*,
G – *Whiteinella paradubia*; **H**, **I** – *Pithonella trejoi*; scale bars values in μm

on the stratigraphic ranges of microfossils such as *Thalmanninella globotruncanoides* and *Thalmanninella brotzeni* of the Taxon Zone of Caron and Premoli-Silva (2007). Biostratigraphic index microfossils are relatively rare as regards recognizing the Cenomanian zones in the study area.

MICROFACIES

Integrated field surveys and petrographic investigations of the Cenomanian Chalajur Formation led to description and interpretation of six microfacies types (Table 1), that comprise dominantly echinoderms (Figs. 6 and 7). Authigenic minerals include glauconite, pyrite (Fig. 5A, B), and sparse phosphate grains (Fig. 6C). Planktonic and small benthic foraminifers (Figs. 6F and 7D) and calcispheres (Fig. 7C), together with red algae, bryozoans, and pelecypods (Figs. 6 and 7), are subsidiary constituents. The only non-skeletal grains comprise intraclasts (Fig. 6D); quartz grains and basaltic and andesitic rock fragments are among extraclasts in the silt- to very fine-grained sand-size fraction (Fig. 7B). Major diagenetic processes and products include neomorphism (Fig. 5A–D), silicification (Fig. 7A), glauconitization (Fig. 7B) and recrystallization. Sedimentary fabrics and structures include bioturbation (Fig. 7D), microscopic erosional surfaces and faint normal grading (Fig. 7E, F). Petrographic investigations reveal that some glauconite grains are skeletal-filling grains dominantly in echinoderms and red algae particles. The general characteristics of the microfacies, numbered 1–6, are summarized in Table 1.

MORPHOLOGY AND COMPOSITION OF GLAUCONITE GRAINS

Microscopic investigation of glauconite grains shows a wide range of yellowish brown, brown, pale green to dark green colours. Scanning electron microscope (SEM) analysis as well as photomicrographs of glauconite grains show typical cauliflower (Fig. 8A) and rosette structures (Fig. 8B), as well as well-developed lamellae in the glauconite grains (Fig. 8C, D). Grain surfaces show rosette morphology of the crystal habit of a glauconite mixed-layer mineral (Fig. 8B).

EDX analysis on four samples and twelve glauconite grains in the lower to middle parts of the Chalajur Formation at the Chalajur section show that O_2, Mg, Al, Si, Ca, Fe, and K are the major constituents (Table 2 and Fig. 9). EDS analysis suggests two ranges of K-content in glauconite grains (Table 2, Figs. 8 and 9B–B2), which varies from 3.15 to 6.94 wt.%. Based on EDS analysis, there is a direct relationship between K_2O and Fe_2O_3 of glauconite grains (Table 2 and Fig. 9).

DISCUSSION

DEPOSITIONAL ENVIRONMENTS AND DEPOSITIONAL MODEL

Eustatic sea-level changes and carbonate production rate seem to have played the main controlling factors in the vertical facies changes (Moosavizadeh et al., 2015); meanwhile, tectonics strongly determined the morphology of the carbonate platforms, and influenced the spatial facies changes as well as thickness variations. Sediments accumulating under tectonically relatively quiescent conditions show more the influence of climate, depositional environments, and diagenesis (Nelson and Hume, 1987; Ando et al., 2015), while depositional geometry is directly dependent on the carbonate production rate and changes in the carbonate factory (e.g., Merino-Tomé et al., 2012).

The data obtained from microfacies analysis and the proportion of carbonate to non-carbonate particles suggest tectonic quiescence during deposition. Based on modest variations in thickness (10 m) and laterally facies distribution (Fig. 10), some differential tectonic subsidence was likely during deposition. Accordingly, we suggest the Cenomanian Chalajur Formation of the north-east Kelardasht and Chalus counties (Fig. 1) was deposited during a relatively stable tectonic regime.

We followed the microfacies and facies belts from one exposure to another with a high degree of confidence. Six microfacies types were identified, using the standard microfacies of the Wilson (1997) and Flügel (2010) (Table 1). Characterization of the microfacies and faunal succession suggest deposition on a carbonate ramp as described by Burchette and Wright (1992), comprising inner-, mid- and outer-ramp facies belts (Table 1) (Figs. 10 and 11).

The main components of the outer-ramp facies belt comprise poorly sorted bioclastic packstone microfacies including echinoderms accompanied by calcispheres and planktonic foraminifers, together with glauconite grains and pyrite (Fig. 5A, B), suggesting deposition in calm and slightly reducing conditions in a low-energy depositional environment below storm wave-base (e.g., Tucker and Wright, 1990; Flügel, 2010; Zeller et al., 2015; Rikhtegarzadeh et al., 2016).

The local occurrence of quartz and silt-sized to very fine-grained sand alkali-basalt and/or andesite extraclasts within the succession studied points to an influx of siliciclastic debris under warm and humid climatic conditions; together with the general tectonic stability, this led to mafic volcanic landmass undergoing varying degrees of chemical weathering in a Cenomanian greenhouse palaeoclimate.

The consistent presence of grain-dominated microfacies with a predominance of echinoderm skeletons associated with planktonic foraminifers and calcispheres (Figs. 5 and 6) suggests deposition in a mid-ramp facies belt (e.g., Flügel, 2010; Salah, 2017). Calcispheres associated with opportunistic planktonic foraminifers such as hedbergellids, heterohelicids, whiteinellids and small benthic foraminifers reflect tropical to subtropical warm waters and eutrophic to mesotrophic conditions in the middle ramp facies belt in which suggest nutrient-enriched surface waters, increased primary productivity, and stressful conditions in the depositional environment (Carson and Crowley, 1993; Dias-Brito, 2000; Omaña et al., 2014) led to a low carbonate production rate.

The mid-ramp facies belt is marked by mixed benthic and planktonic foraminifers and calcispheres associated with a few intraclasts (Fig. 6C, D), echinoderms, pelecypods and bryozoans, together with quartz and sparse volcanic rocks as well as faint lamination (Fig. 6E, F). Based on the constituent grains and stratigraphic position, this microfacies type belongs the middle-ramp facies belt corresponding to a ~30–50 m wa-

Table 1

Microfacies types of the Cenomanian Chalajur Formation

Microfacies Type	Description of microfacies and components	Interpretation
Microfacies 1: Lithoclastic-bioclastic wackestone	This microfacies occurs in thin- to medium-bedded greenish grey beds only in the base of the succession, which overlies mafic volcanic rocks in the study area. The microfacies comprises mainly basalt clasts associated with benthic foraminifers, red algae, echinoderms, pelecypods, and sparse shell fragments (Fig. 6A).	Occurrence of basalt lithoclasts at the beginning of the succession signifies a flooding surface above the nonconformity surface. The basalt extraclasts suggest a substrate composed of mafic volcanics. Unaltered alkali-basalt rocks suggest minimal chemical weathering and short transport (Kavoosi, 2013). Lithoclastic bioclastic wackestone suggests reworking of skeletal grains and basaltic substrate during relative sea-level rise.
Microfacies 2: Echinoderm-bioclastic grainstone	Echinoderm-bioclastic grainstone predominates near the upper part of the sedimentary succession (Fig. 4D). Echinoderms are the dominant constituents, as well as small benthic foraminifers and red algae (Fig. 6B). The main diagenetic processes and products are syntaxial calcite cement overgrowths on the echinoderm particles (Fig. 6B).	The grainstone facies reflects deposition in a high-energy shoal environment. The low diversity of small benthic foraminifers is attributed to stress in the depositional environment related to physicochemical parameters (Jasionowski et al., 2012). Colonization of the sea floor by filter-feeding organisms, such as echinoderms and bryozoans most likely exerted an influence on stabilization of sediment due to rapid cementation under low production rate (Della Porta et al., 2003). Lack of sedimentary structures can be attributed to restricted conditions.
Microfacies 3: Sandy glauconitic-bioclastic packstone	Characterized by thin- to medium-bedded greenish grey limestone and embedded marl. Autochthonous particles comprise glauconite and a few phosphatic grains (Figs. 6C and 7B). Quartz and basalt to andesite extraclasts are in the silt- to very fine-grained sand fraction (Figs. 6C and 7B). Glauconite grains retain the shape of host volcanic extraclasts and skeletal grains (red algae and echinoderms). The microfacies yields a rich assemblages of skeletal grains comprising mainly echinoderms associated with bryozoans and pelecypods. Major diagenetic processes and products include silicification, glauconitization (Fig. 7A, B) and neomorphism.	Echinoderms are an important constituent of the marine community in the Cenomanian of the study area. The predominance of echinoderms suggest establishment of echinodermal bioherms and/or banks in the study area inferred from echinodermal mound geometry at the Petilingeh section (Figs. 1 and 2). The echinoderm particles were broken and reworked before deposition. Local occurrence of quartz and silt-sized to very fine-grained sand alkali basalt and/or andesitic extraclasts points to an influx of siliciclastics into the depositional environment during sea-level rise and/or climatic perturbations. In spite of a low carbonate production rate, the lack of micritic envelopes suggests low and even absent bacterial activity in the depositional environment (e.g., Olchowy and Krajewski, 2020). The association of echinoderms, planktonic foraminifers and calcispheres; together with glauconite grains and siliciclastics, are characteristic of a stressful environment with low sedimentation rate.
Microfacies 4: Glauconitic bioclastic-intraclastic packstone	This microfacies occurs as commonly greenish grey thin-bedded limestones. Intraclasts and echinoderms are the predominant particles (Fig. 6D). Subsidiary constituents are planktonic foraminifers, calcispheres, red algae, glauconite and sparse phosphate grains. Sedimentary structures include erosional surfaces and faint normal grading (Fig. 7C–F). Syntaxial calcite cement overgrowths are well-developed on the echinoderm components (Fig. 7C, E).	A mixture of benthic and planktonic foraminifers suggests deposition at depths of ~30–50 m (Smith et al., 2006; Baldermann et al., 2017). Echinoderms typically accompany the red algae and bryozoans in the mid-ramp facies belt (Adams et al., 1967; Fornos and Ahr, 2006). Fine-grained intraclasts accompanied by faint normal grading suggest distal storm deposits. Authigenic glauconites correspond to deposition during a major eustatic sea-level rise with low sedimentation rate. Intraclasts comprising the calcispheres are observed at the Pol-e Zoghal section, which is compatible with a deeper palaeogeographic position during deposition.
Microfacies 5: Glauconitic bioclastic packstone	This microfacies comprises greenish grey well-bedded limestone. Several beds make individual packages separated by interbedded marl. The faunal assemblage is marked by a predominance of echinoderm fragments (Fig. 6E). Other constituents are calcispheres, planktonic foraminifers, bryozoans, red algae, and glauconite grains	The high-diversity fauna documents normal salinity. The consistent presence of a grain-dominated microfacies with generally poor sorting of skeletal grains including the planktonic foraminifers, together with very rare platform derived grains, as well as glauconite grains, suggest a low carbonate production rate and deposition in a low- to moderate-energy depositional environment below storm wave base (e.g., Flügel, 2010; Zeller et al., 2015).
Microfacies 6: Echinoderm-bioclastic packstone	This consists of thin- to medium-bedded limestone without evidence of high-energy sedimentary structures. Echinoderm skeletons (Fig. 6F) associated with calcispheres and *Heterohelix* are the main components. Planktonic foraminifers (Fig. 6F) are subsidiary skeletal grains. Pyrite and glauconite have filled the chambers of some planktonic foraminifers (Fig. 5A, B).	Co-occurrence of echinoderms and planktonic foraminifers as well as calcispheres suggests deposition in a low-energy environment below storm wave base on an outer ramp. Calcispheres reflect eutrophic to mesotrophic conditions accompanied by high nutrient supplies as well as high primary productivity and surface warm waters (e.g., Carson and Crowley, 1993; Dias-Brito, 2000; Wendler et al., 2002), which resulted in very low carbonate production rate. The occurrence of pyrite and glauconite suggest suboxic-anoxic conditions at the water-sediment interface during and/or after deposition

ter-depth (Adams et al., 1967; Fornos and Ahr, 2006; Smith et al., 2006; Baldermann et al., 2017). Accompanying fine- to medium-grained intraclasts are composed of calcispheres, together with very fine-grained basalt clasts (Figs. 5D and 6C), reflect storm events. The scarcity of red algae as a subordinate component signifies a lack of hard substrate, which enhanced

reworking of unconsolidated carbonates by storms (e.g., Westphal et al., 2010).

We propose too an inner-ramp facies belt based on the stratigraphic pattern of the microfacies, the occurrence of benthic foraminifers and bioclastic grainstone and/or bioclastic packstone comprising echinoderms, red algae, and benthic foraminifers as well as a lack of glauconite grains (Figs. 9 and 10).
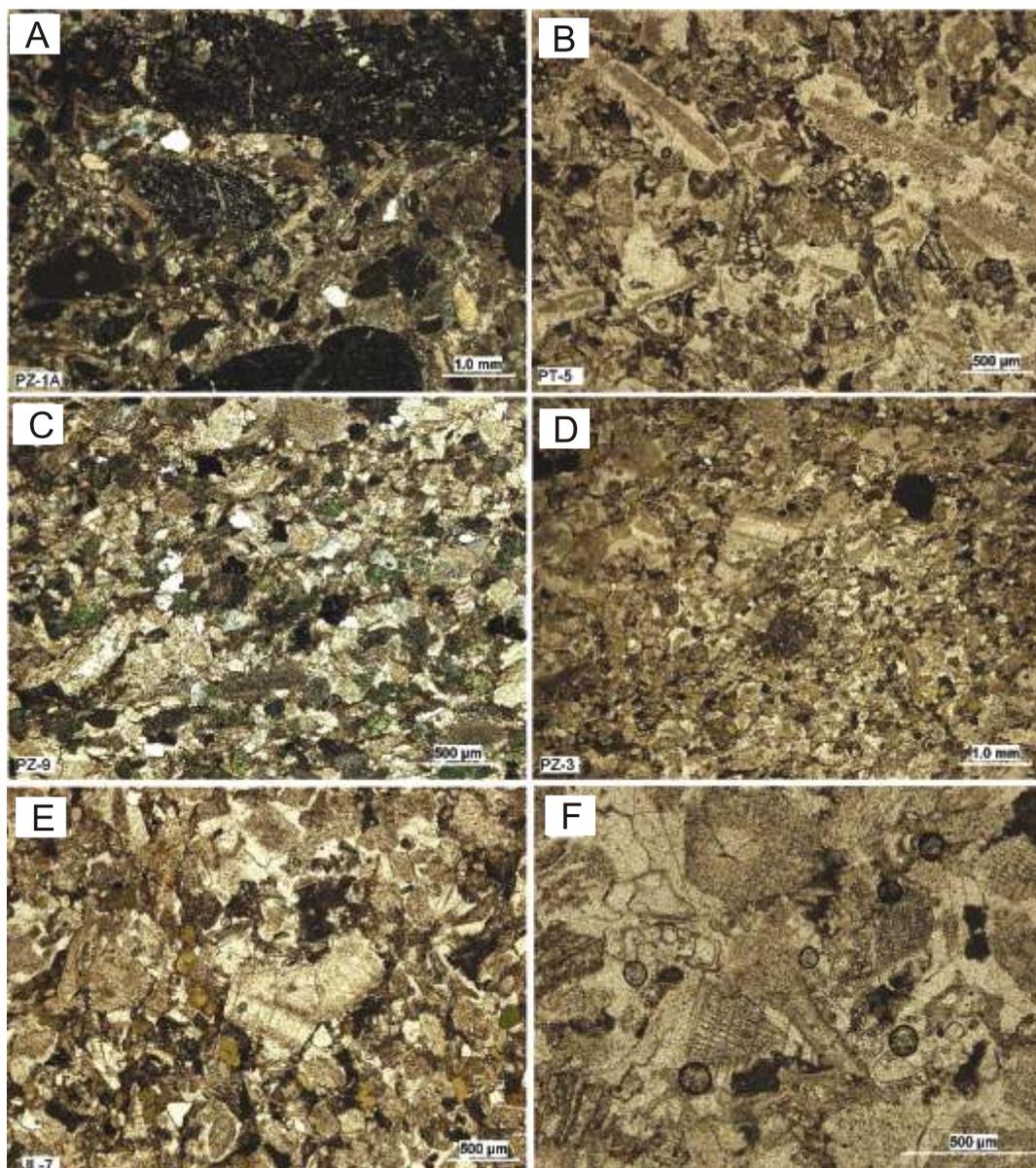
Fig. 6. The microfacies identified in the succession studied

A – photomicrograph of a lithoclastic bioclastic wackestone; basalt extraclasts associated with echinoderm and pelecypod fragments, and sparse glauconite grains in the base of the formation, crossed polars (XPL); **B** – photomicrograph of echinoderm bioclastic grainstone composed predominantly of echinoderms associated with small benthic foraminifers and sparse red algae, plane polarized light (PPL); **C** – photomicrograph of sandy glauconitic bioclastic packstone that includes skeletal and non-carbonate grains such as glauconite grains, extraclasts and quartz; the skeletal grains are composed mainly of echinoderms with sparse pelecypods, XPL; **D** – glauconitic bioclastic intraclastic packstone microfacies composed of echinoderms, pelecypods, intraclasts, extraclasts and glauconite grains, XPL; **E** – photomicrograph of glauconitic bioclastic packstone with echinoderm and pelecypod components and glauconite grains, XPL; **F** – echinoderm bioclastic packstone microfacies composed mainly of echinoderms and planktonic foraminifers, PPL

Based on the regional geological context, the succession studied has a limited distribution in the South Caspian Basin, surrounded to the south and north-west by mafic volcanic islands (Barrier et al., 2018). We infer that deposition of the Chalajur Formation took place on a mafic volcanic rock substrate (Fig. 11). Occurrence of basalt extraclasts in some of microfacies suggest that the study area was surrounded by volcanic land masses (Fig. 11).

CONTROLLING FACTORS OF THE HETEROZOAN CARBONATES

This study reports Cenomanian heterozoan carbonates (James, 1997) in the north-central Alborz Mountains. We identified a heterozoan association with a light-independent, suspension-feeding, and heterotrophic fauna including echinoderms,
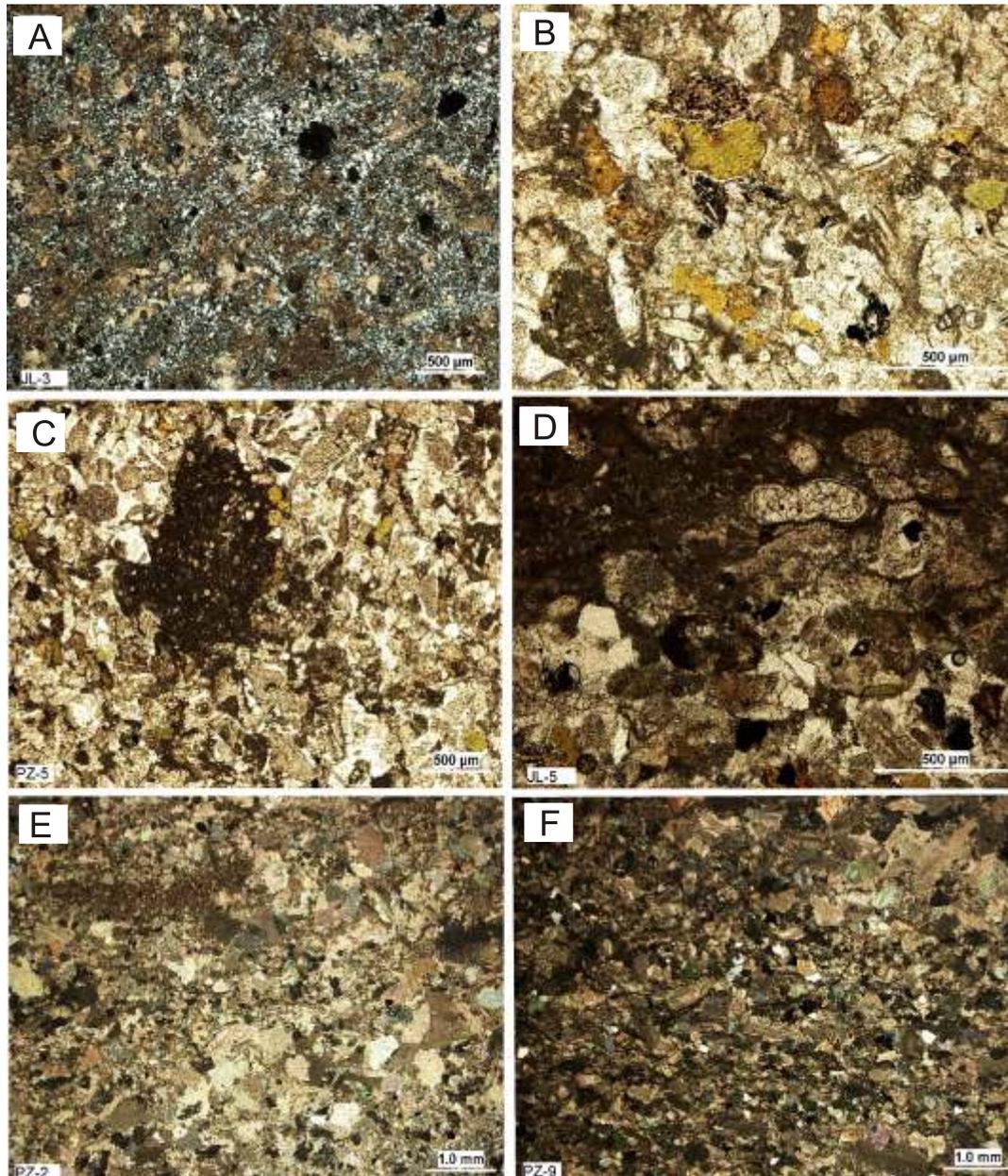
**Fig. 7. Photomicrographs of some microfacies, sedimentary fabrics, and diagenetic textures
of the Cenomanian Chalajur Formation**

A – silicification in a bioclastic packstone composed of echinoderms and pelecypods, XPL; **B** – authigenic glauconite in a sandy glauconite bioclastic packstone; volcanic extraclasts were replaced by glauconite and the glauconite grains retain the shape and morphology of the host grains, which signifies an authigenic origin, XPL; **C** – intraclast includes calcispheres providing evidence of distal storm deposits on a mid-ramp, XPL; **D** – bioturbation in a bioturbated bioclastic packstone comprising echinoderms, planktonic foraminifers, calcispheres and a few glauconite grains, PPL; **E**, **F** – microscopic erosional surfaces and faint normal grading in glauconitic bioclastic intraclastic packstone and sandy glauconitic bioclastic packstone microfacies, XPL

calcispheres, planktonic foraminifers, bryozoans and pelecypods (foramol association), together with a lack of aragonitic skeletal- and non-skeletal grains such as calcareous green algae and ooid grains (Figs. 6, 7 and 10).

Heterozoan carbonates develop as the result of high nutrient content, mobile substrate, environmental and trophic conditions, sea-water chemistry, and temperature (e.g., Knöerich, 2005; Pomar et al., 2005; Lukasik and James, 2006; García-Hidalgo et al., 2012).

The echinoderm remains have considerable significance to the heterozoan carbonates in the study area (Figs. 6, 7 and 10), and can be related to environmental conditions and climate. Microfacies analysis indicates that the echinoderms are accompanied by different fossils related to a wide range of depositional environments from the inner-, mid- to outer-ramp facies belts (Figs. 10 and 11). The consistent predominance of echinoderm components suggests no considerable changes in sea-water salinity (cf. Peryt et al., 2016). Primary factors in
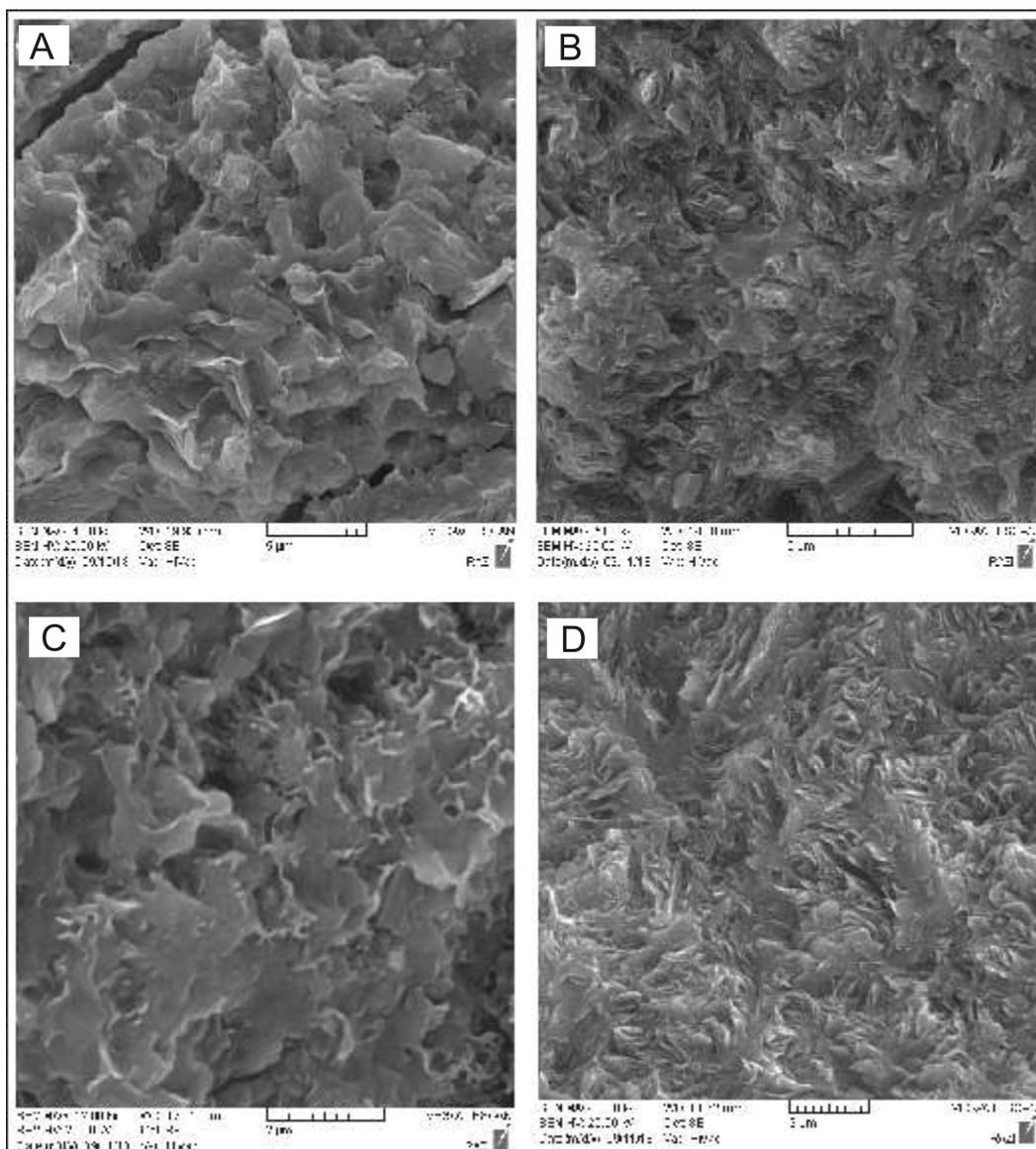
Fig. 8. High-resolution SEM images of glauconite grains

A – scanning electron photomicrograph representing the cauliflower morphology of the glauconite; **B** – surfaces of the grain show rosette structure and/or morphology, which suggest a mixed-layer mineral habit of the glauconite grain; **C**, **D** – well-developed lamellae of glauconite grains indicating authigenic origin; for location of samples see Table 2 and Figure 10 (in the column of samples and weathering profile)

echinoderm taphonomy were palaeoenvironmental conditions and disarticulation modes (e.g., Brett et al., 1997; Hunter and Underwood, 2009). The distribution and preservation potential of echinoderms have been attributed to many factors including nutrient availability, substrate type, and turbulence as well as water depths of >50–70 m (Nebelsick, 1995, 1996; Smith et al., 2006).

The disarticulated and somewhat abraded nature of the echinoderm skeletons, together with planktonic foraminifers and calcispheres, suggest that they were transported and redeposited in the depositional environment. Our results are in line with the idea that echinoderms were both autochthonous and allochthonous (e.g., Krajewski et al., 2020). A lack of complete echinoderms suggests that all of them were transported to some degree before deposition.

The association of calcispheres, echinoderms, planktonic foraminifers, and opportunistic Tethyan organisms, suggests warm- and normal salinity conditions, nutrient-enriched, and $CaCO_3$-rich surface waters of marginal seas (Hart, 1991; Dias-Brito, 2000). These heterozoan carbonates, forming in warm waters during the hot greenhouse Cenomanian, raise the question of their spatial and temporal controls.

An enhanced rate of the sea-level rise accompanied by large-scale igneous provinces across the globe, with high global temperatures, led to an increase in weathering rate of mafic volcanic rocks, which introduced colder, fresh and nutrient-rich waters into the depositional environment, resulting in eutrophic to mesotrophic conditions (Carson and Crowley, 1993; Charbonnier et al., 2018a; Percival et al., 2018; Banerjee et al., 2019; Jafarzadeh et al., 2020; Baioumy et al., 2021).
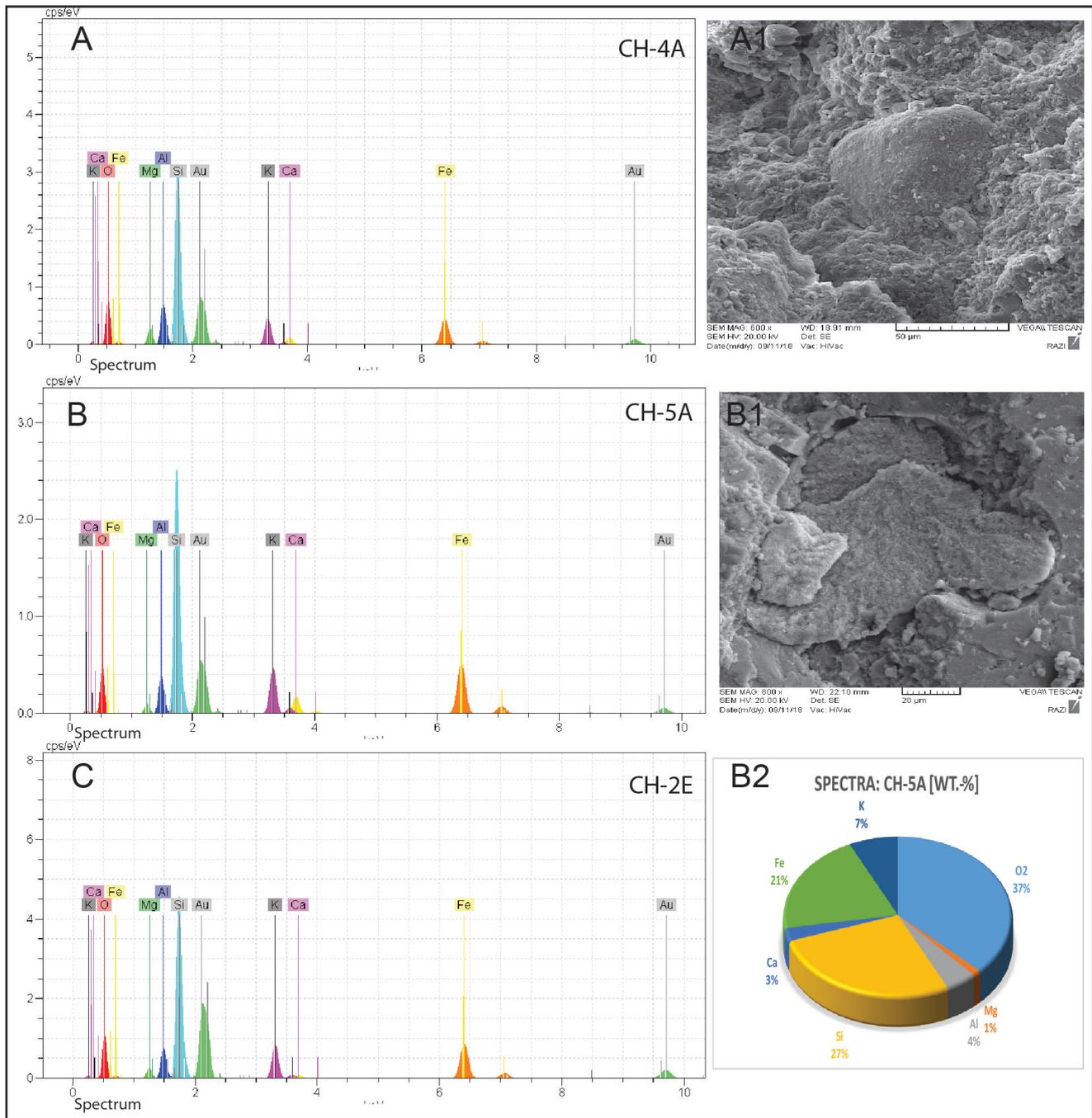
Fig. 9. Energy dispersive spectroscopy (EDS) results and scanning electron photomicrographs of some glauconite grains; EDX analysis of four samples and twelve glauconite grains of the Chalajur Formation from the Chalajur section show that O$_2$, Mg, Al, Si, Ca, Fe, and K are the major constituents

A – high K content of glauconite grain indicates a high degree of maturation; glauconite is compatible with Fe- and K-rich, and Al-rich glauconite; **A1** – scanning electron photomicrograph of glauconite and its EDS, indicating a Fe-rich glauconite grain; **B1** – scanning electron photomicrograph of glauconite and its EDS, indicating a Fe-rich glauconite grain; **B, B2** – high K content, as well as the microtexture, indicates an evolved and mature glauconite grain; **C** – EDS of a glauconite grain; for location of samples see Table 2 and Figure 10 (in the column of samples and weathering profile)

Mafic volcanic eruptions around the world were the main mechanism plausibly responsible for high atmospheric carbon dioxide levels then and a primary control on the global climate, which led to high nutrient levels (e.g., Nichols, 2009). Abundant mafic volcanic rocks and alkali basalts related to extensional movements have been reported from the South Caspian Basin as well as in and around the Indian Ocean during the Cenomanian (Bitschene et al., 1992; Barrier et al., 2018).

A combination of petrographic investigations (Figs. 7B and 8) and EDS analyses (Table 2 and Fig. 9) suggest an overall nutrient-dependent environment in combination with relative sea-level rise and warm-water control on the end-member

Representative EDS data for some glauconite grains from the Chalajur section

Samples	Grains	Elements [wt.%]							
		O2	Mg	Al	Si	Ca	Fe	K	Ti
JL-2	CH-2C	33.98	1.45	3.62	19.26	1.29	14.47	5.02	
	CH-2E	25.18	1.19	3.13	17.18	0.44	18.90	5.34	
JL-3	CH-3B	29.40	1.55	4.12	22.93	1.08	18.90	6.15	
	CH-3C	34.59	1.51	3.86	21.00	2.90	15.15	5.52	
	CH-3E	36.40	1.68	4.19	22.24	0.99	16.32	6.44	
JL-4	CH-4A	30.72	2.44	5.64	23.94	1	13.29	3.54	
	CH-4B	32.44	1.17	3.29	17.08	1.60	14.30	6.94	1.02
	CH-4C	28.67	1.65	3.78	17.03	3.42	9.90	3.15	
	CH-4D	21.89	1.43	4.00	19.72	2.28	11.42	4.90	
JL-5	CH-5A	32.34	1.04	3.82	23.28	2.3	17.81	6.15	
	CH-5B	24.04	0.73	3.61	18.82	7.22	17.55	6.03	
	CH-5B	16.60	2.04	5.20	25.72	1.80	17.03	5.12	0.41

Results show two ranges of potassium content of glauconite grains, varying from 3.15 to 6.94 wt.%

heterozoan carbonates of the study area. Our conclusion is supported by the nature of the biogenic assemblages as well as by authigenic pyrite (Fig. 5A, B), glauconite and sparse phosphate grains in the Cenomanian Chalajur Formation.

Microfacies analysis suggests palaeoecological stress during deposition inferred from stenohaline and eutrophic/euryhaline species including echinoderms and calcispheres, indicating nutrient-rich warm water (e.g., Hart, 1991; Carson and Crowley, 1993; Dias-Brito, 2000; Bensong et al., 2008; Westphal et al., 2010).

These conditions resulted in establishment eutrophic conditions, which led to a decrease in carbonate production rate on mid- to outer-ramp facies belts. Accordingly, nutrient-rich and eutrophic conditions contributed to the generation of heterozoan carbonates, despite the hot greenhouse conditions during the Cenomanian.

GLAUCONITIZATION AND PRESERVATION

Two main hypotheses may be invoked to explain the formation and preservation of glauconite grains in the succession studied:
 – sourcing of glauconites from an older rock (reworked),
 – a marine authigenic origin.

A reworking source is unlikely, given the lack of abraded glauconite grains or evidence of their transport (Figs. 5–7).

The nature and frequency distribution of minerals in sedimentary successions is mainly controlled by climate, tectonics, depositional environment, and diagenesis (Nelson and Hume, 1987). Based on our petrographic and SEM studies, we propose an authigenic origin for glauconite grains (Figs. 8 and 9). Petrographic investigations show that the glauconite infills skeletal grains (dominantly echinoderms and red algal particles, Fig. 12), are mainly authigenic, and developed contemporaneously and/or very soon after deposition. Our studies show that some of the echinoderm and red-algal skeletons as well as volcanic extraclasts were replaced by glauconite, while glauconite grains retain the shape and morphology of the host grains (Figs. 7B and 12). This signifies an authigenic origin under low sedimentation and slightly reducing conditions (Fig. 5A, B).

There is a direct relationship between the occurrence and/or frequency of glauconite grains and siliciclastic influx (Figs. 6C, E and 7B, C). Glauconite grains are scattered throughout the Chalajur Formation. In some layers glauconite grains are generally associated with a varying admixture of quartz and mafic extraclasts (silt- to very-fine-grained sand size, Figs. 6C, E and 7B, C). Therefore, the abundance of glauconite grains may have resulted from a combination of enhanced weathering of nearby mafic volcanic landmasses, which provided a sufficient Al, Fe, Si, Mg, and K cations supply (Table 2), and the establishment of reducing conditions. The state of oxidation, accompanied by enough Fe supply in the depositional environment, led to high-Mg calcite components such as echinoderms and red algae which turned into ferroan calcite, while preserving the skeletal structure (Fig. 12; Richter, 1983).

Based on morphology, mineralogy, microfacies, and faunal association together with depositional environment, the glauconite grains are autochthonous. Glauconite grains typically form in conditions of major eustatic sea-level rise, low sedimentation rate, and global warming as well as sub-oxic conditions (Carson and Crowley, 1993; Jafarzadeh et al., 2020; Baioumy et al., 2021). Oxygen-deficiency and oxygen-depletion in the depositional environment facilitate the mobility and fixation of Fe into the glauconite structure at the water-sediment interface (Banerjee et al., 2019).

Cretaceous pelagic facies in SE Spain contain large numbers of glauconite grains that mimic the shape of the bioclasts (Jimenez-Millan et al., 1998), and a high content of glauconite grains has been reported from the Upper Cretaceous succession in the South Island of New Zealand (McConchie and Lewis, 1980). Field and published data (Jafarzadeh et al., 2020) sug-
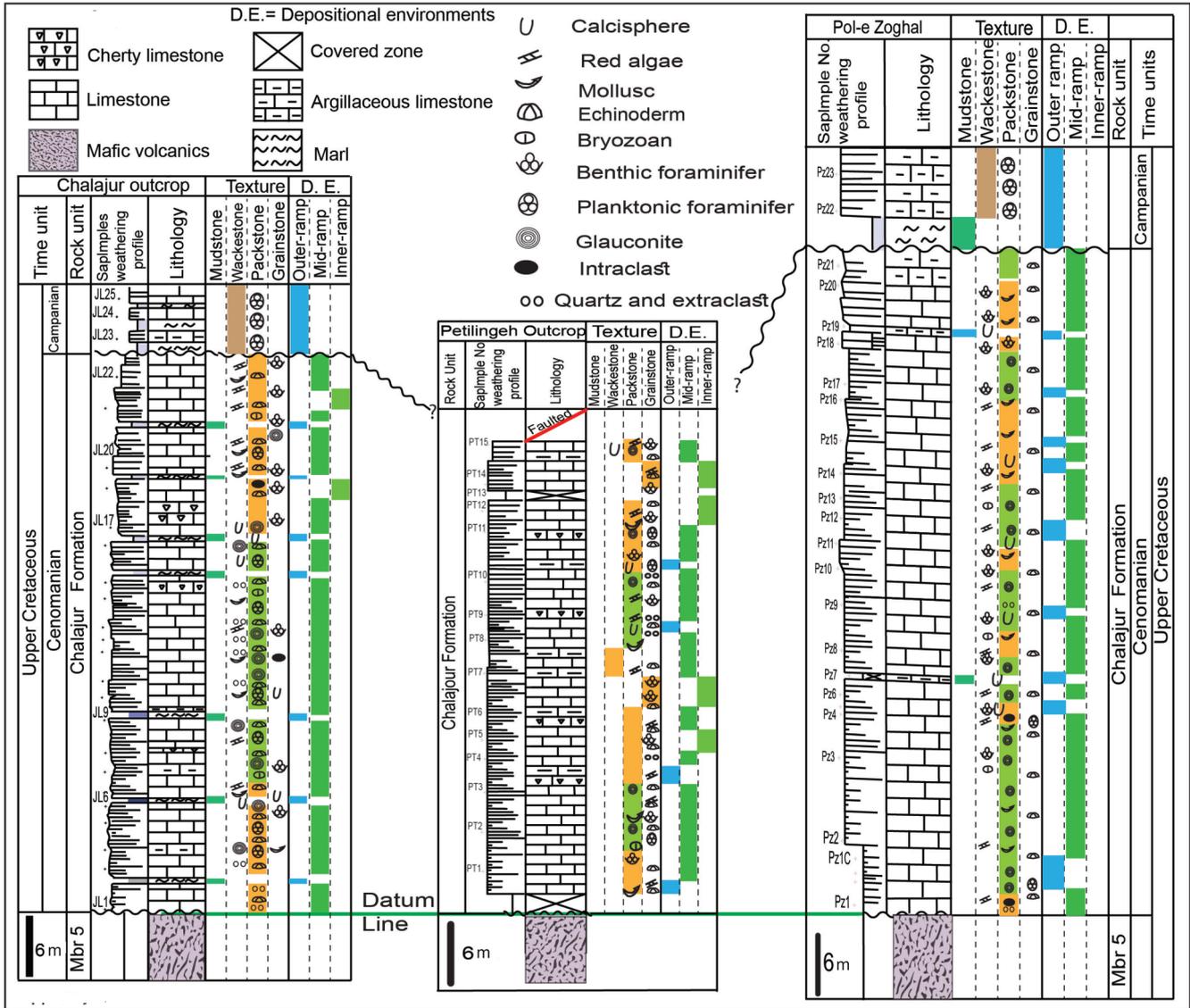
Fig. 10. General view and a correlation chart of the Cenomanian Chalajur Formation at the Chalajur, Petilingeh, and Pol-e Zoghal sections

The correlation chart includes age, sample numbers, thickness, weathering profile, lithology, and sedimentary structures (physical and biological), textures, depositional environments associated with main carbonate and non-carbonate grains, together with underlying and overlying boundaries (see Figs. 1 and 2 for location)

gest that the Cenomanian succession of the study area is continuous laterally and possibly correlates with the Cenomanian Aitamir Formation in the Kopeh Dagh Basin. In the north-central Alborz, glauconitic limestone persist, while the Cenomanian Aitamir Formation is a glauconitic sandstone and shale. The mid-Upper Cenomanian glauconitic limestone of the south-east Esfahan area in the Central Iranian Basin, with a total thickness of ~4 m, has been interpreted as a condensed zone (Kennedy et al., 1979; Hairapetian et al., 2018).

The terrestrial influx from intense chemical weathering of mafic volcanic landmasses led to higher nutrient levels and a supply of ions, especially Fe, unfavourable for carbonate production but providing suitable conditions for authigenic glauconites to form and grow.

Palaeoecological stress related to high-nutrient conditions associated with a lower state of oxidation in the depositional environment led to low production of skeletal carbonates, allowing

time for authigenic minerals such as glauconite to grow. The association of abundant echinoderms, planktonic foraminifers, and calcispheres in the glauconitic well-bedded chert-bearing limestone of the Chalajur Formation (Figs. 10 and 12) is characteristic of a stressful environment with low sedimentation rate related to relative sea-level rise, with fresh- and nutrient-enriched waters, a semi-confined microenvironment within the substrate, and reduced oxygen levels (Odin and Matter, 1981; Odin and Fullagar, 1988; Dias-Brito, 2000; Nichols, 2009; Omaña et al., 2014).

The cauliflower structure (Fig. 8A), boxwork and rosette structures (Fig. 8B), and well-developed lamellae of the evolved glauconite grains (Fig. 8C, D), indicate an authigenic origin (e.g., Oddin and Matter, 1981). EDS analysis revealed glauconite grains with two ranges of potassium content (Table 2, Figs. 8 and 9B–B2), varying from 3.15 to 6.94 wt.%. Based on the EDS analysis, there is a direct relationship between K_2O and
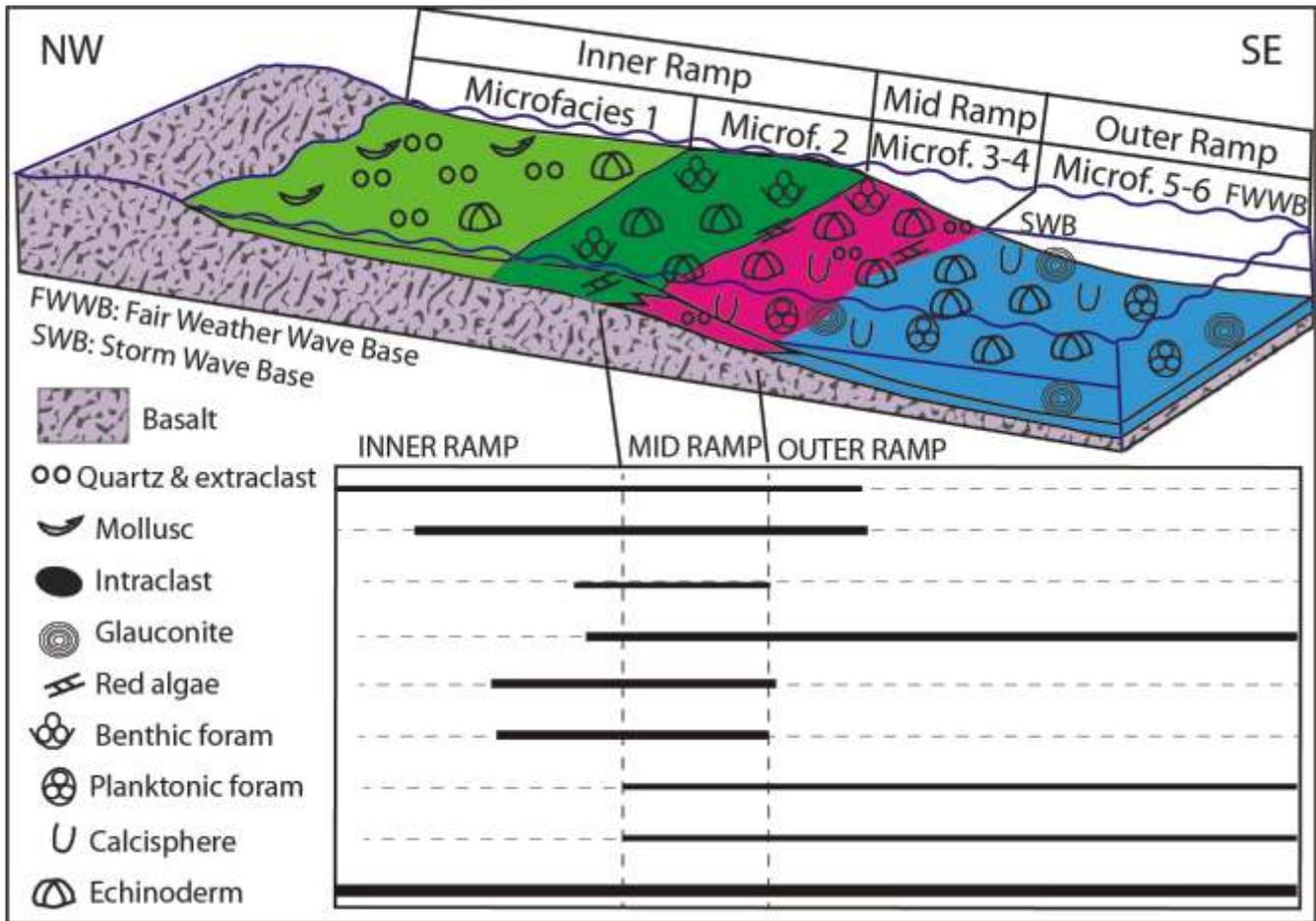
Fig. 11. The proposed depositional model of the Cenomanian Chalajur Formation in the study area

The depositional model is a carbonate ramp that comprises the inner-, mid- and outer-ramp facies belts
in which carbonate deposited on a basalt substrate

Fe_2O_3 (Table 2 and Fig. 9). A high content of K (5 wt.%) of glauconite grains (Fig. 9), indicates a high degree of maturation. The green and brown colours of glauconite grains are compatible with Fe- and K-rich glauconites, respectively (Table 2, Figs. 6C, E, 7B, C, F, 9 and 12). The high content of K, as well as the micro-texture (Figs. 8, 9B–B2, 12A, D), is in line with an evolved and mature glauconite. By contrast, light brown and pale green colours (Fig. 12B, C) comprising a low content of K (<5 wt.%; Table 2), indicates a low degree maturation of glauconite grains.

Green glauconite grains are Fe- and K-rich and mature (Figs. 6C, E, 7B, C, F, 9 and 12), while Al-rich glauconite grains have brown colour (Table 2). The maturity depends on the residence time of grains near to the sediment-water interface (Banerjee et al., 2012). A high maturity of glauconite grains is compatible with a long residence time for glauconite grains at the sediment-water interface under a low sedimentation rate (Banerjee et al., 2016a, b).

CONCLUSIONS

Our detailed field and petrographic investigations on the Cenomanian carbonates have resulted in the recognition of six microfacies, related to the inner-, mid- and outer-ramp facies belts of a carbonate ramp. Heterozoan carbonates were deposited on a carbonate ramp under eutrophic conditions. A predominance of echinoderms associated with calcispheres, planktonic foraminifers, a lack of calcareous green algae or ooids, a low carbonate production rate together with a high content of glauconite grains, and a prevalent high-Mg calcite mineralogy, characterize temperate heterozoan carbonates.

Palaeoecological stress related to high-nutrient conditions, associated with a lower state of oxidation in the depositional environment and a supply of required ions especially Fe, led to low production of skeletal carbonates while providing suitable conditions for authigenic glauconite grains to form and grow.

Our petrographic investigation shows a direct relationship between the proportion of glauconite grains and periods of sea-level rise inferred from siliciclastic influx into the depositional environment. Petrographic and SEM studies reveal that glauconite-filling skeletal grains retain the shape and morphology of the host grains which signifies an authigenic origin under low sedimentation and slightly reducing conditions. The cauliflower, boxwork, and rosette structures associated with well-developed lamellae of evolved glauconite grains indicate an authigenic origin. The EDS analysis revealed glauconite grains with two ranges of potassium content. High contents of K (5 wt.%) as well as the micro-texture is in line with evolved and mature glauconite grains.
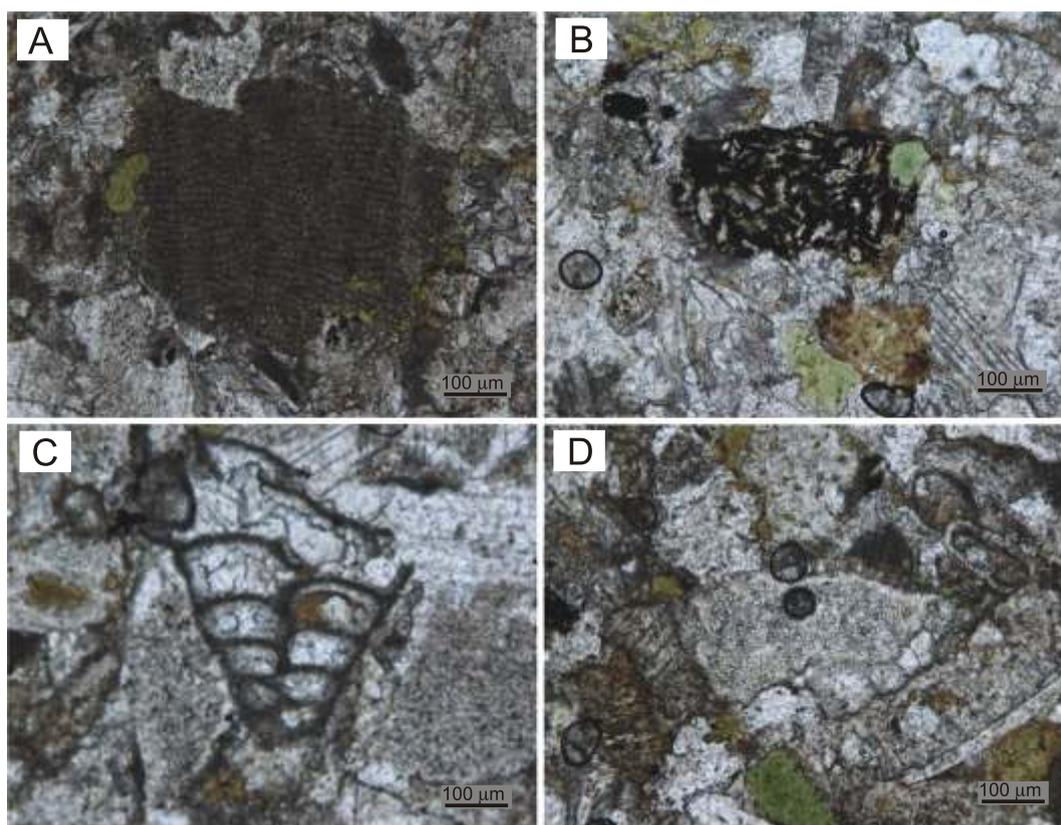
Fig. 12. Photomicrographs of carbonate samples with glauconite grains that are mainly authigenic in origin

A – glauconite infilling red algae; the glauconite retain the shape and morphology of the red algal grains, which signifies an authigenic origin, XPL; **B** – some echinoderms and chambers of planktonic foraminifers have been filled by glauconite and pyrite; co-occurrence of glauconite and pyrite suggests a low sedimentation rate and slightly reducing conditions, XPL; **C** – chambers of benthic foraminifera and echinoderm skeleton infilled with glauconite; **D** – green and brown colours of glauconite grains are compatible with Fe- and K-rich glauconite grains, respectively; high content of K, as well as the micro-texture, is consistent with evolved and mature glauconite

Our findings are compatible with an overall nutrient-rich conditions and palaeoecological stress related to relative sea-level rise and eutrophic conditions, which contributed to generation of heterozoan carbonates despite the hot green-house conditions during the Cenomanian in the north-central Alborz Mountains.

REFERENCES

Abbaspour-Tehrani, A., 2014. Microfacies analysis and depositional environments of the glauconitic limestone at Pol-e-Zoghal and Nargessan outcrop section, NE Kelardasht, N Iran (in Persian with English summary). MSc. Thesis, Shahroud Free University.

Adams, T.D., Khalili, M., Khosravi, Said, A., 1967. Stratigraphic significance of some oligosteginid assemblages from Lurestan Province, southwest Iran. Micropaleontology, **3**: 55–67.

Alavi, M., 1996. Tectonostratigraphic synthesis and structural style of the Alborz mountain system in Iran. Journal of Geodynamics, **21**: 1–33.

Allen, M.B., Ghassemi, M.R., Shahrabi, M., Qorashi, M., 2003. Accommodation of Late Cenozoic oblique shortening in the Alborz range, northern Iran. Journal of Structural Geology, **24**: 659–672.

Ando, A., Huber, B.T., MacLeod, K.G., Watkins, D.K., 2015. Early Cenomanian "hot greenhouse" revealed by oxygen isotope record of exceptionally well preserved foraminifera from Tanzania. Paleoceanography, **30**: 1556–1572.

Baioumy, H., Ahmed Salim, A.M., Ahmed, N., Maisie, M., Al-Kahtany, K., 2021. Upper Cretaceous-Upper Eocene mud-dominated turbidites of the Belaga Formation. Sarawak (Maly-

sia): 20 Ma of paleogeographic, paleoclimate and tectonic stability in Sundaland. Marine and Petroleum Geology, **126**: 104897.

Baldermann, A., Dietzel, M., Mavromatis, V., Mittermayr, F., Warr, L.N., Wemmer, K., **2017.** The role of Fe on the formation and diagenesis of interstratified glauconite-smectite and illite-smectite: a case study of Upper Cretaceous shallow-water carbonates. Chemistry Geology, **453**: 21–34.

Banerjee, S., Chattoraj, S.L., Saraswati, P.K., Dasgupta, S., Sarkar, U., 2012a. Substrate control on formation and maturation of glauconites in the Middle Eocene Harudi Formation, western Kutch, India. Marine and Petroleum Geology, **30**: 144–160.

Banerjee, S., Bansal, U., Pande, K., Meena, S.S., 2016a. Compositional variability of glauconites within the Upper Cretaceous Karai Shale Formation, Cauvery Basin, India: implications for evaluation of stratigraphic condensation. Sedimentary Geology, **331**: 12–29.

Banerjee, S., Bansal, U., Thorat, A.V., 2016b. A review on palaeogeographic implications and temporal variation in glaucony composition. Journal of Palaeogeography, **5**: 43–71.

Banerjee, S., Farouk, S., Nagm, E., Choudhury, T.R., Meena, S.S., 2019. High Mg-glauconite in the Campanian Duwi Formation of Abu Tartur Plateau, Egypt and its implications. Journal of African Earth Sciences, **56**: 12–25.

Bansal, U., Banerjee, S., Pande, K., Ruidas, D.K., 2020. Unusual seawater composition of the Late Cretaceous Tethys imprinted in glauconite of Narmada basin, central India. Geological Magazine, **157**: 233–247.

Barrier, E., Vrieyynck, B., Brouillet, J.-F., Brunet, M.-F., 2018. Paleotectonic reconstruction of the Central Tethyan realm. Darious Programme, Map 9, Cenomanian.

Bensong, J., James, N.P., Beauchamp, B., 2008. Carbonate deposition during a time of Mid-latitude Ocean cooling: Early Permian subtropical sedimentation in the Sverdrup Basin, Arctic Canada. Journal of Sedimentary Research, **78**: 2–15.

Berra, F., Zanchi, A., Mattei, M., Nawab, A., 2007. Late Cretaceous transgression on a Cimmerian high (Neka Valley, Eastern Alborz, Iran): a geodynamic event recorded by glauconitic sands. Sedimentary Geology, **199**: 189–204.

Bitschene, P.R., Holmes, M.A., Breeza, J., 1992. Composition and origin of Cr-rich glauconitic sediments from the southern Kerguelen Plateau (site 748). Proceedings of the Ocean Drilling Program, Scientific Results, **120**: 113–134.

Brett, C.E., Moffat, H.A., Taylor, W.L., 1997. Echinoderm taphonomy, taphofacies, and lagerstätten. Paleontological Society Papers, **3**: 147–190.

Burchette, T.P., Wright, V.P., 1992. Carbonate ramp depositional systems. Sedimentary Geology, **79**: 3–57.

Caron, M., Premoli-Silva, I., 2007. New description of the rotaliporid species Brotzeni and globotruncanoides Sigal, 1948 based on re-examination of type material. Rivista Italiana di Paleontologia e Stratigrafia, **113**: 525–530.

Carson, G.A., Crowley, S., 1993. The glauconite-phosphate association in hardgrounds: examples from the Cenomanian of Devon, southwest England. Cretaceous Research, **14**: 69–89.

Cartier, E.T., 1971. Die Geologie des unteren Chalus-Tals, Zentral-Alborz, Iran. Mineralogical and Geological Institute ETH. University of Zürich, N.R.

Charbonnier, G., Boulila, S., Spangenberg, J.E., Adatte, T., Follmi, K.B., Laskar, J., 2018a. Obliquity pacing of the hydrological cycle during the Oceanic Anoxic Event 2. Earth and Planetary Science Letters, **499**: 266–277.

Della Porta, G., Kenter, J.A.M., Bahmonde, J.R., Immenhauser, A., Villas, E., 2003. Microbial boundstone dominated carbonate slope (Upper Carboniferous, N Spain). Facies, lithofacies distribution and stratal geometry. Facies, **49**: 175–208.

Dias-Brito, D., 2000. Global stratigraphy, palaeobiogeography and palaeoecology of Albian–Maastrichtian pithonellid calcispheres: impact on Tethys configuration. Cretaceous Research, **21**: 315–349.

Dunham, R.J., 1962. Classification of carbonate rocks according to depositional texture. AAPG Memoir, **1**: 108–121.

Egan, S.S., Mosar, J., Brunet, M.-F., Kangarli, T., **2009**. Subsidence and uplift mechanisms within the South Caspian Basin: insights from the onshore and offshore Azerbaijan region. Geological Society Special Publications, **312**: 219–240.

Ezoji, N., 2002. Microstratigraphy of the Upper Cretaceous sediments in the northeast Kelardasht (in Persian with English summary). MSc. Thesis, Shahid Beheshti University, Tehran.

Flügel, E., 2010. Microfacies of Carbonate Rocks. Springer, Berlin, Heidelberg.

Fornos, J.J., Ahr, W.M., 2006. Present-day temperate carbonate sedimentation on the Balearic Platform, western Mediterranean: compositional and textural variation along a low-energy isolated ramp. Geological Society Special Publications, **25**: 571–584.

Fürsich, F.T., Wilmsen, M., Syed-Emami, K., Cecca, F., Mjidifard, M.R., **2005**. The upper Shemshak Formation (Toarcian–Aalenian) of the eastern Alborz (Iran): biota and palaeoenvironments during a transgressive–regressive cycle. Facies, **51**: 365–384.

Fürsich, F.T., Wilmsen, M., Syed-Emami, K., Majidifard, M.R., **2009a**. The Mid-Cimmerian tectonic event (Bajocian) in the Alborz Mountains, Northern Iran: evidence of the break-up unconformity of the South Caspian Basin. Geological Society Special Publications, **312**: 189–203.

Fürsich, F.T., Wilmsen, M., Seyed-Emami, K., Majidifard, M.R., **2009b**. Lithostratigraphy of the Upper Triassic-Middle Jurassic Shemshak Group of northern Iran. Geological Society Special Publications, **312**: 129–160.

García-Hidalgo, J.F., Barrosso-Barcenilla, F., Gil-Gil, G., Martínez, R., Pons, J.M., Segura, M., 2012. Stratal, sedimentary and faunal relationships in the Coniacian 3rd-order sequence of the Iberian Basin, Spain. Cretaceous Research, **34**: 268–283.

Guest, B., Guest, A., Axen, G., 2007. Late Tertiary tectonic evolution of northern Iran: a case for simple crustal folding. Global and Planetary Change, **58**: 435–453.

Hairapetian, V., Wilmsen, M., Ahmadi, A., Shojaei, Z., Berensmeier, M., Majidifard, M.R., 2018. Integrated stratigraphy, facies and correlation of the upper Albian-lower Turonian of the Esfahan area (Iran): unravelling the conundrum of the so-called "Glauconitic Limestone". Cretaceous Research, **90**: 391–411.

Hart, M.B., 1991. The Late Cenomanian calcisphere global bioevent. Proceedings of the Ussher Society, **7**: 413–417.

Huber, B.T., MacLeod, K.G., Watkins, D.K., Coffin, M.F., 2018. The rise and fall of the Cretaceous hot greenhouse climate. Global and Planetary Change, **167**: 1–23.

Hunter, A.W., Underwood, C.J., 2009. Palaeoenvironmental control on distribution of crinoids in the Bathonian (Middle Jurassic) of England and France. Acta Palaeontologica Polonica, **54**: 77–98.

Jafarzadeh, M., Choudhury, T.R., Roy, T., Taheri, A., Banerjee, S., Jafarian, A., 2020. Glauconite within Albian-Cenomanian Aitamir Formation, Kopet-Dagh Basin, northeastern Iran: origin and implications of Cretaceous seawater. Arabian Journal of Geosciences, **13**: 12–36.

James, N.P., 1997. The cool-water carbonate depositional realm. SEPM Special Publication, **56**: 1–23.

Jasionowski, M., Peryt, D., Peryt, T.M., 2012. Neptunian dykes in the Middle Miocene reefs of western Ukraine: preliminary results. Geological Quarterly, **56** (4): 881–894.

Jimenez-Millan, J., Molina, J.M., Nieto, F., Nieto, L., Ruiz-Ortiz, P.A., 1998. Glauconite and phosphate peloids in Mesozoic carbonate sediments (Eastern Subbetic zone, Betic Cordilleras, SE Spain). Clay Mineralogy, **33**: 547–559.

Kangi, A., Aryaei, A.A., Maassoomi, A., 2010. Synsedimentary deformation in Member 2 of the Mila Formation in the Central Alborz Mountains. Arabian Journal of Geosciences, **3**: 33–39.

Kavoosi, M.A., 2013. Evidence for volcanic activity in the Upper Permian Nar Member of the Dalan Formation, southeast Iran. In: Permo-Triassic Sequence of the Arabian Plate (ed. M. Poppelrieter): 147–162. EAGE Publications, Houten, the Netherlands.

Kavoosi, M.A., Ezoji, N., 2018. Facies, depositional environments, and sequence stratigraphy analysis of the upper Barremian-

-lower Aptian carbonates in the northeast Kelardasht, N Iran. Journal of African Earth Sciences, **147**: 228–242.

Kennedy, W.J., Chahida, M.R., Djafarian, M.A., 1979. Cenomanian cephalopods from the glauconitic limestone southeast of Esfahan, Iran. Acta Palaeontologica Polonica, **24**: 3–50.

Knöerich, A.C., 2005. Investigations on the importance of early diagenetic processes for the mineralogical stabilization and lithification of heterozoan carbonate assemblages (Oligo-Miocene, Maltese Islands and Sicily). PhD Thesis, Institut für Geowissenchaften, Universität Potsdam.

Krajewski, M., Ferre, B., Salamon, M.A., 2020. Cyrtocrinids (Cyrtocrinida, Crinoidea) and other associated crinoids from the Jurassic (Kimmeridgian–Tithonian)–Cretaceous (Berriasian–Barremian) of the Carpathian Foredeep basement (western Ukraine). Geobios, **60**: 61–77.

Lukasik, J., James, N.P., 2006. Carbonate sedimentation, climate change and stratigraphic completeness on a Miocene cool-water epeiric ramp, Murray Basin, South Australia. Geological Society Special Publications, **255**: 217–244.

Mattei, M., Cifelli, F., Alimohammohadzadian, H., Rashid, H., Winkler, A., Sagnotti, L., 2017. Oroclinal bending in the Alborz Mountains (Northern Iran): new constraints on the age of South Caspian subduction and extrusion tectonics. Gondwana Research, **42**: 13–28.

McConchie, D.M., Lewis, D.W., 1980. Varieties of glauconite in Late Cretaceous and Early Tertiary rocks of the South Island of New Zealand, and new proposals for classification. New Zealand Journal of Geology and Geophysics, **23**: 413–437.

Merino-Tomé, Ó., Della Porta, G., Kenter, J.A.M., Verwers, K., Harris, P., Adams, E.W., Playton, T., Corrochano, D., 2012. Sequence development in an isolated carbonate platform (Lower Jurassic, Djebel Bou Dahar, High Atlas, Morocco): influence of tectonics, eustacy and carbonate production. Sedimentology, **59**: 118–155.

Moosavizadeh, M.A., Mahboubi, A., Moussavi-Harami, R., Kavoosi, M.A., Schlagintweit, F., 2015. Sequence stratigraphy and platform to basin margin facies transition of the Lower Cretaceous Dariyan Formation (northeastern Arabian Plate, Zagros fold-thrust belt, Iran). Bulletin of Geosciences, **91**: 145–172.

Nebelsick, J., 1995. Uses and limitations of actuopalaeontological investigations on echinoids. Geobios, **18**: 329–336.

Nebelsick, J., 1996. Biodiversity of shallow-water Red Sea echinoids: implications for the fossil record. Journal of the Marine Biological Association, **76**: 185–194.

Nelson, C.S., Hume, M.H., 1987. Paleoenvironmental controls on mineral assemblages in a shelf sequence: Te Kuiti Group, South Auckland, New Zealand. New Zealand Journal of Geology and Geophysics, **30**: 343–362.

Nichols, G., 2009. Sedimentology and Stratigraphy. Second edition. John Wiley and Sons.

Odin, G.S., Matter, A., 1981. De glauconiarum origine. Sedimentology, **28**: 611–641.

Odin, G.S., Fullagar, P.D., 1988. Geological significance of the glaucony facies. Developments in Sedimentology, **45**: 295–332.

Olchowy, P., Krajewski, M., 2020. Lower Kimmeridgian facies and sedimentary succession of a shallow-water coated-grain-dominated carbonate ramp of the northern peri-Tethyan shelf: an example from the Radomsko Folds (central Poland). Geological Quarterly, **64** (4): 969–987.

Omaña, L., Torres, J.R., Doncel, R.L., Alencáster, G., Caballero, I.L., 2014. A pithonellid bloom in the Cenomanian-Turonian boundary interval from Cerritos in the western Valles–San Luis Potosí platform, Mexico: paleoenvironmental significance. Revista Mexicana de Ciencias Geologicas, **31**: 28–44.

Percival, L.M.E., Jenkyns, H.C., Matter, T.A., Dickson, A.J., Batenburg, S.J., Ruhl, M., Hesselbo, S.P., Barclay, R., Jarvis, I., Robinson, S., Woelders, L., 2018. Does large igneous province volcanism always perturb the mercury cycle? Comparing the records of oceanic anoxic event 2 and the

end-Cretaceous to other Mesozoic events. American Journal of Science, **318**: 799–860.

Peryt, D., Peryt, T.M., Halas, S., Raczy ski, P., 2016. Microfacies, foraminifers and carbon and isotopes in a basinal section of the Zechstein Limestone (Wuchiapingian): Bonikowo 2 borehole, western Poland. Geological Quarterly, **60** (4): 827–839.

Petrizzo, M.R., Caron, M., Premoli-Silva, I., 2015. Remarks on the identification of the Albian/Cenomanian boundary and taxonomic clarification of the planktonic foraminifera index species globotruncanoides, brotzeni and tehamaensis. Geological Magazine, **152**: 521–536.

Pomar, L., Gill, E., Obrador, A., Ward, W.C., 2005. Facies architecture and high-resolution sequence stratigraphy of an upper Cretaceous platform margin succession. Southern Central Pyrenees, Spain. Sedimentary Geology, **175**: 339–365.

Purser, B.H., 1973. The Persian Gulf Holocene. Carbonate Sedimentation and Diagenesis in a Shallow Epicontinental Sea. Springer, Heidelberg.

Richter, D.K., 1983. Calcareous ooids: a synopsis. In: Coated Grains (ed. T.M. Peryt): 71–99. Springer, Berlin, Heidelberg.

Rikhtegarzadeh, M., Vaziri, S.H., Aleali, M., Amiri Bakhtiar, H., Jahani, D., 2016. Microbiostratigraphy, microfacies and depositional environment of the Sarvak Formation in Bibi Hakimeh Oil Field (well no. 29), southwest Iran. International Journal of Geography and Geology, **5**: 194–208.

Robert, A.M.M., Letouzey, J., Kavoosi, M.A., Sharham, Sh., Jaume Vergés, Aghababai, A., 2014. Structural evolution of the Kopeh Dagh fold-and-thrust belt (NE Iran) and interactions with the South Caspian Sea Basin and Amu Darya Basin. Marine and Petroleum Geology, **57**: 68–87.

Rudmin, M., Banerjee, M., Mazurov, A., 2017. Compositional variation of glauconites in Upper Cretaceous–Paleogene sedimentary iron-ore deposits in south-eastern western Siberia. Sedimentary Geology, **355**: 20–30.

Salah, A.H., 2017. Oligosteginid assemblages of basinal limestone succession in Ismaelawa section, Kurdistan region, north Iraq. Diyala Journal for Pure Sciences, **13**: 183–196.

Salvador, A., 1994. International stratigraphic guide. A guide to stratigraphic classification, terminology, and procedure (second edition). Co-published by the International Union of Geological Sciences and the Geological Society of America.

Shahidi, A., Barrier, E., Brunet, M.-F., Saidi, A., 2011. Tectonic evolution of the Alborz in Mesozoic and Cenozoic (in Persian with English summary). Scientific Quarterly Journal, Geoscience, **21**: 201–212.

Smith, A.B., Monks, N.E.A., Gale, A.S., 2006. Echinoid distribution and sequence stratigraphy in the Cenomanian (Upper Cretaceous) of southern England. Proceedings of the Geologists' Association, **117**: 207–217.

Taheri, J., Fürsich, F.T., Wilmsen, M., 2009. Stratigraphy, depositional environments and geodynamic significance of the Upper Bajocian Bathonian Kashafrud Formation, NE Iran. Geological Society Special Publications, **312**: 205–218.

Tucker, M.E., Wright, V.P., 1990. Carbonate Sedimentology. Blackwell Scientific Publication.

Vahdati Daneshmand, F., Karimkhani, A., Karimi, H.R., 2001. The Geological Map of Chalus (in the scale of 1:100 000). The Geological Survey of Iran, Tehran.

Wendler, J., Gräfe, K.-U., Willems, H., 2002. Palaeoecology of calcareous dinoflagellate cysts in the mid-Cenomanian boreal realm: implications for the reconstruction of palaeoceanography of the NW European shelf sea. Cretaceous Research, **23**: 213–229.

Westphal, H., Halfar, J., Freiward, A., 2010. Heterozoan carbonates in subtropical to tropical settings in the present and past. International Journal of Earth Science, **99**: 153–169.

Wilmsen, M., Fürsich, F.T., Seyed-Emami, K., Majidifard, M.R., Taheri, J., 2009. The Cimmerian orogeny in northern Iran:

tectono-stratigraphic (evidence from the foreland. Terra Nova, **21**: 211–218.

Wilson, J.L., 1997. Carbonate depositional environments and diagenesis. Geophysical Developments Series, **6**: 9–29.

Yassaghi, A., Naeimi, A., 2010. Structural analysis of the Gachsar sub-zone in central Alborz range: constrain for inversion tectonics followed by the range transverse faulting. International Journal of Earth Science, **99**: 1237–1249.

Yilmaz, I.O., Cook, T.D., Hosgor, I., Wagreich, M., Rebman, K., Murray, A.M., 2018. The upper Coniacian to upper Santonian drowned Arabian carbonate platform, the Mardin-Mazidag area,

SE Turkey. Sedimentological, stratigraphic, and ichthyofaunal records. Cretaceous Research, **84**: 153–167.

Zanchi, A., Zanchetta, S., Berra, F., Mattei, M., Garzanti, E., Molyneux, S., Navab, A., Sabouri, J., 2009. The Eo-Cimmerian (Late? Triassic) orogeny in North Iran. Geological Society Special Publications, **312**: 31–35.

Zeller, M., Verwer, K., Eberli, G.P., Massaferro, J.L., Schwarz, E., Spalletti, L., 2015. Depositional controls on mixed carbonate-siliciclastic cycles and sequences on gently inclined shelf profiles. Sedimentology, **62**: 2009–2037.